

Nitrous Oxide Vibrational Energy Relaxation Is a Probe of Interfacial Water in Lipid Bilayers

Logan R. Chieffo,[†] Jeffrey T. Shattuck,[†] Eric Pinnick,[‡] Jason J. Amsden,[‡] M. K. Hong,[‡] Feng Wang,[†] Shyamsunder Erramilli,^{*,§} and Lawrence D. Ziegler^{*,†}

Department of Chemistry, Department of Physics, Department of Biomedical Engineering and the Photonics Center, Boston University, 590 Commonwealth Avenue, Boston, MA 02215

Received: February 11, 2008; Revised Manuscript Received: July 7, 2008

Ultrafast infrared spectroscopy of N₂O is shown to be a sensitive probe of hydrophobic and aqueous sites in lipid bilayers. Distinct rates of VER of the ν_3 antisymmetric stretching mode of N₂O can be distinguished for N₂O solvated in the acyl tail, interfacial water, and bulk water regions of hydrated dioleoylphosphatidylcholine (DOPC) bilayers. The lifetime of the interfacial N₂O population is hydration-dependent. This effect is attributed to changes in the density of intermolecular states resonant with the ν_3 band ($\sim 2230\text{ cm}^{-1}$) resulting from oriented interfacial water molecules near the lipid phosphate. Thus, the N₂O VER rate becomes a novel and experimentally convenient tool for reporting on the structure and dynamics of interfacial water in lipids and, potentially, in other biological systems.

Introduction

Interfacial water molecules play an essential role in biological activity¹ contributing to the specificity and structural organization of lipid, protein, and nucleic acid components in living cells. For example, the self-assembly and dynamical behavior of phospholipid bilayers is dependent on the extent of hydration and solvation properties of the aqueous environment. Experimental probes of the static and dynamic properties of phospholipid–water regions include NMR,² small-angle X-ray scattering, neutron scattering,^{3,4} and nonlinear spectroscopic methods such as time-resolved fluorescence,^{5,6} coherent anti-Stokes Raman scattering (CARS) microscopy,⁷ and photon echo measurements.⁸ Molecular dynamics (MD) simulations of hydrated phospholipid systems have also been carried out.^{9–11} Experimental and simulation results suggest that the interfacial water structure and dynamics are perturbed by the polar head groups and the nanoconfined boundary conditions of the phospholipid bilayer.

Furthermore, a variety of time-resolved infrared measurements have been applied to reverse-micelle systems, which may be viewed as model membrane systems.¹² Many of the experiments utilize small solute molecules to probe the reverse-micelle environments as a function of hydration. Sando et al.¹³ reported the vibrational energy relaxation (VER) of the azide ion in these systems, while Fayer and co-workers have utilized the OD hydroxyl stretch of HOD to monitor the orientational relaxation,¹⁴ VER, and vibrational echoes¹⁵ in reverse micelles. Several pump–probe studies have looked directly at the OH stretching mode of H₂O to interrogate the energy-transfer dynamics of nanoconfined aqueous environments.^{16,17} All of these studies show similar results; the dynamics are slowed inside of these reverse micelle systems, and as hydration is

increased, the responses become faster approaching the bulk values. These results are generally interpreted as a change in the hydrogen-bonding network of the nanoconfined water molecules resulting in elongated dynamics. Two-color experiments performed by the Bakker group were able to directly observe a change in the relaxation mechanism of the OH stretch due to nanoconfinement.¹⁷

The VER of small molecules in condensed phases is well-known to be solvent-dependent.¹⁸ Here, we show that the VER of the anesthetic gas nitrous oxide (N₂O) measured by ultrafast infrared spectroscopy provides a novel, sensitive, and experimentally convenient tool for studying the structure and dynamics of interfacial water molecules in lipid bilayers and, potentially, in other biological systems. The antisymmetric stretch (ν_3) of the neutral linear triatomic molecule N₂O is observed at 2224 cm^{-1} in the gas phase.^{19–22} The ν_3 band is especially attractive for IR spectroscopic studies of biological systems because it has a large extinction coefficient ($\sim 1.5 \times 10^3\text{ M}^{-1}\cdot\text{cm}^{-1}$) and its frequency falls in a spectral region ($\sim 2215\text{--}2230\text{ cm}^{-1}$) that is removed from absorptions due to most protein, nucleic acid, and other biomolecule fundamentals.

Using the vibrational lifetime of N₂O as an experimental probe of biological hydration water molecules offers several advantages as compared to other spectroscopic techniques. The weak dipole moment of N₂O (0.166 D)²³ allows both polar and nonpolar solvent environments of a complex biological structure to be probed within a single experiment (vide infra). The ν_3 vibrational lifetime (10^{-12} to 10^{-11} s) is on the order of water residence times in the biological systems of interest and is convenient for direct comparison with MD simulations. The small size of N₂O makes it a less perturbing probe of inherent structures than molecular dyes often used as spectroscopic probes, as in time-dependent fluorescence Stokes shift or photon echo measurements. Finally, a sensitive probe of the molecular details of N₂O sites in hydrated lipids and proteins could provide considerable insight for understanding the molecular mechanism of general anesthetic action.^{24,25} Both lipid membrane and the more widely accepted protein-based models of anesthetic action have been proposed for N₂O.^{24,26–29} Static Fourier transform

* To whom correspondence should be addressed. Phone: 617-353-1271; fax: 617-353-9393; e-mail: shyam@bu.edu (Shyamsunder Erramilli). E-mail: lziegler@bu.edu (Lawrence Ziegler).

[†] Department of Chemistry and the Photonics Center.

[‡] Department of Physics.

[§] Department of Physics and Department of Biomedical Engineering and the Photonics Center.

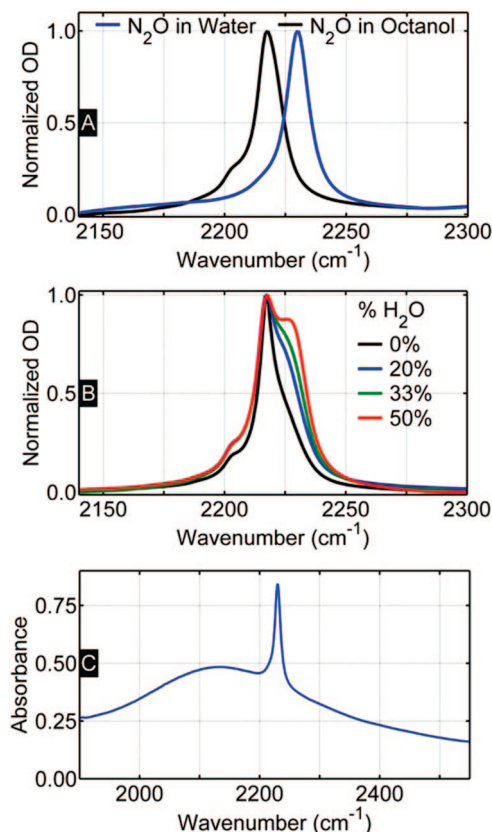


Figure 1. (A) Normalized FTIR spectra of the ν_3 vibrational band of N_2O in water and octanol. (B) FTIR of N_2O in DOPC–water bilayers with increasing percentage of water composition by weight. (C) FTIR spectrum of N_2O (10 atm) in liquid water in the region of the ν_3 transition. This N_2O transition overlaps both the bend–libration combination band and a continuum absorption due to overtones and combinations of low-frequency intermolecular modes of H_2O .

infrared (FTIR) studies have led to a proposal that interfacial hydrogen bonding near lipid head groups plays a role in anesthetic interactions.³⁰ Techniques are required for identifying and characterizing the active sites for N_2O binding in membrane structures.

Static FTIR studies of N_2O solvated in a variety of biomolecular systems have been carried out previously. The ν_3 band is red-shifted from its gas-phase value to $2218 \pm 1 \text{ cm}^{-1}$ in a hydrocarbon-rich environment and is blue-shifted to $2230 \pm 1 \text{ cm}^{-1}$ in water^{31,32} as shown in Figure 1A for N_2O in octanol and in water, respectively. The small shoulder at 2203 cm^{-1} in the N_2O octanol FTIR spectrum is due to a hot band absorption.¹⁹ In addition to the ν_3 frequency solvent dependence, we have found the N_2O ν_3 vibrational lifetimes to be very different in these two solvents: 55 ps in octanol³³ and 9 ps in H_2O .³⁴ The solubility of N_2O in octanol (and olive oil) has been correlated with the potency of anesthetic action according to the Meyer–Overton observations.^{24,25} The 9 ps lifetime is very similar to that of the asymmetric stretch of another triatomic, CO_2 , in aqueous solution which has been reported as 10 ps.³⁵

The results of VER studies of N_2O dissolved in model lipid membranes consisting of hydrated bilayers of dioleoylphosphatidylcholine (DOPC), a neutral zwitterionic phospholipid with an 18-carbon diacyl tail, are described here. Neutron diffraction shows that ~ 12 water molecules/lipid molecule are needed to form a monolayer of water around the DOPC polar head group.³ As DOPC is hydrated, the thickness of the aqueous layer between the acyl chains increases and, at room temper-

ature, lamellar bilayers ordered in the liquid crystalline L_α phase are formed. Beyond ~ 27 water molecules/lipid, an excess water point is reached,³ where pools of bulk water accumulate, and the polar head groups are separated by a $\sim 4 \text{ nm}$ aqueous region. Thus, hydrated lipid bilayers offer a variety of solvation environments for N_2O .

Experimental Procedures

Ultrafast Pump–Probe Spectroscopy. Femtosecond pulses tuned to the N_2O ν_3 absorption band were generated in a series of nonlinear down conversions. A 1 kHz regenerative Ti:Sapphire amplifier (Spectra-Physics) was used to pump an optical parametric amplifier. The resulting signal and idler undergo difference frequency mixing in a $300 \mu\text{m}$ silver gallium sulfide (AgGaS_2) crystal to provide 130 fs pulses centered at 2200 cm^{-1} . A 1:2 reflective telescope enlarged and collimated the IR beam to provide a tighter focal spot size at the sample ($100 \mu\text{m}$ diameter). The beam was split into pump and probe arms using a 50–50 calcium fluoride (CaF_2) beam splitter (ISP Optics). A pair of 2 in. retro-reflectors (Prosystem), mounted on computer-controlled translation stages with 10 nm resolution (Melles Griot), provided the relative delay between pump and probe. The polarization between the pump and probe beams was set to the magic angle using a pair of CaF_2 holographic wire grid polarizers (ThorLabs). The energies of the pump and probe pulses were $1 \mu\text{J}$ and $0.5 \mu\text{J}$, respectively. The beams were focused into the sample and were recollimated using a pair of unprotected gold-coated off-axis parabolic mirrors (Janos Technology, focal length = 101.6 mm). After the sample, the probe beam was focused by a CaF_2 lens onto the entrance slit of a 0.150 m monochromator (Acton) equipped with a 150 grooves/mm grating blazed at $4 \mu\text{m}$. A 32-element mercury cadmium telluride (MCT) liquid-nitrogen-cooled linear array detector (Infrared Associates, Inc.) was placed at the focal plane of the monochromator. The response from the detector was sent to a boxcar integrator and was digitized using a multichannel laser pulse spectroscopy system (Infrared Systems Development Corporation) controlled with LabView software.

Sample Preparation. Lyophilized 1,2-dioleoyl-*sn*-glycero-3-phosphocholine (DOPC) was purchased from Avanti Polar Lipids, Inc. A specific volume of deionized water was added using a Drummond microdispenser to a weighed sample of lyophilized DOPC to obtain the specified hydration by mass percent water. Hydrated DOPC forms lipid bilayers in the L_α phase at room temperature. These are randomly oriented liquid crystalline domains. The hydrated DOPC was placed between two uncoated 2 mm thick CaF_2 windows. The path length was set by a $25 \mu\text{m}$ Teflon spacer. The windows were then placed inside a home-built stainless steel IR pressure cell and were pressurized with 10 atm of N_2O (Linde Gas, 99% purity). At this pressure, the absorbance at the peak of the N_2O ν_3 absorption is ~ 0.50 OD, and the concentration of N_2O in the lipid reached 130 mM. The IR cell was left for 24 h to allow full equilibration of N_2O with the lipid bilayer. Static FTIR spectra were recorded at 2 cm^{-1} resolution with a Nicolet FTIR spectrometer equipped with a liquid-nitrogen-cooled MCT detector.

Global Fitting Analysis. A global fitting procedure³⁶ was used to analyze dispersed pump–probe data. The time dependence of the pump-induced IR absorbance change, ΔS , at each of the simultaneously observed ν_j probe frequencies ($j = 1–32$) is fit to a weighted sum of exponential damped spectral components represented by $\Delta S(\nu_j, t) = \sum_{i=1}^N A_i(\nu_j) e^{-t/\tau_i} + A_{\text{long}}(\nu_j)$. Each of the N components with distinct lifetimes τ_i is

represented by a decay associated spectrum (DAS) $A_i(\nu_j)$. $A_{\text{long}}(\nu_j)$ is a constant which represents the sub-picosecond heating contribution to the signal that decays on a much longer time scale (ms) than the time range of these measurements (120 ps). The hydrated lipid pump–probe responses were modeled as a sum of two exponential decays for samples below the excess water point and a sum of three exponential decays plus A_{long} for samples above the excess water point. The first point for the data analysis corresponds to a pump–probe delay of 200 fs to avoid contamination because of coherence coupling effects. The bleach contribution of the acyl chain solvated N_2O overlaps the absorptive contribution of the hydrated N_2O preventing unambiguous global analysis of the blue side of the transient signal. Thus, only global analysis of the bleach side of the dispersed probe response is reported here. A consistency check of the global analysis was performed by fitting to single frequency data.

Molecular Dynamic Simulations. Molecular dynamics simulations have previously been used to study vibrational spectra and VER of small molecules in reverse micelles³⁷ or at water–air surfaces.³⁸ Lipid–water interfaces are different from reverse micelles because of the lack of curvature and from water–air interfaces because of the presence of head groups. Reliable simulation of the energy relaxation process requires quantum treatment of vibrational energy levels, accurate quantum mechanical intermolecular forces, and coupling with intramolecular vibrational relaxation. We postpone such a study to a full theoretical paper. In this work, we probed how the presence of lipid bilayers perturbs the hydrogen bond network of the water molecules and how such perturbation affects the intermolecular vibrational density of states. There have been numerous studies of water in lipid bilayers.^{11,39,40} To gain further insight into water arrangement around phospholipid bilayers, high-resolution molecular dynamics (MD) simulations of fully hydrated 1-palmitoyl-2-oleoyl-*sn*-glycero-3-phosphocholine (POPC) were carried out. High-quality force fields for this system are available, and the POPC and DOPC interfacial water structure is expected to be very similar for the two lipids since the polar head groups and lipid phases (L_α) at the experimental and simulation conditions are identical. Most existing studies of hydrated lipid bilayers are based on nonpolarizable rigid water models. The OH bond in a rigid water is not able to stretch when a hydrogen bond with a lipid head group is formed. Furthermore, nonpolarizable water models will not be able to model head group water molecules reliably since the average dipole moment for water close to head groups is expected to be different from that of bulk water molecules. Using polarizable water molecules requires a significant amount of CPU time and is cost prohibitive for large-scale simulations. In this work, we chose to use a recently developed high-quality flexible water model.⁴¹ The dipole moment of a flexible water molecule can change as a result of flexible water geometry, and thus a flexible water model is also polarizable. While the polarizability of a flexible water model is unrealistically small, the model offers a significant improvement over nonpolarizable rigid models.

Molecular dynamics simulations were carried out using the Gromacs package.^{42–44} A cuboid periodic box containing 128 POPC molecules and 2460 water molecules was used. The POPC force field is taken from the Tieleman group.⁴⁵ The flexible water model we used is the SPC/Fw model.⁴¹ The membrane is parallel to the X – Y plane with an area density of 0.548 nm^{-2} . The z dimension of the box is 6.54 nm. The initial configuration was equilibrated for 1 ns in a constant particle number, normal pressure, surface area, and temperature (NPAT)

ensemble and then was equilibrated in the canonical ensemble for 1 ns. Statistics were then accumulated for 1 ns in a canonical ensemble by saving configurations once every 20 fs for structural properties and once every 2 fs for power spectra calculations. A time step of 0.5 fs was used. The Nosé–Hoover thermostat was used to maintain the system temperature at 310 K. Electrostatic interactions were treated exactly using the particle mesh Ewald method.⁴⁶ A calculation of the oxygen and hydrogen spectral density of SPC/Fw water as a function of distance from the phosphocholine head group for the frequency range from 0 to 1000 cm^{-1} resulting from the Fourier transform of the velocity autocorrelation function was also carried out. More details on this calculation, intended to show that the water vibrational density of states is altered in the phospholipid interfacial region, are given in the Supporting Information (see Figure S9).

Results

Static Absorption Spectra. FTIR spectra of N_2O (10 atm) in DOPC bilayers at varying degrees of hydration (% H_2O by weight) are shown in Figure 1B and exhibit multiple absorption components. The 2218 cm^{-1} peak is assigned to N_2O in the hydrophobic acyl tail regions of DOPC. An absorption band near 2230 cm^{-1} becomes increasingly evident at higher hydration levels because of N_2O in aqueous solvated regions of the bilayer associated with the polar head groups, and in bulk liquid water pools above the excess water point. The N_2O ν_3 absorption band overlaps a broad, weak H_2O absorption feature due to the L_2 libration–bending combination band, $\nu_B + \nu_L$, centered at 2130 cm^{-1} and the continuum of higher order intermolecular states of liquid water as shown in Figure 1C. These water absorption contributions have been subtracted from the N_2O solution spectra shown in Figure 1A and 1B.

Pump–Probe Measurements. One-color dispersed pump–probe measurements of the ν_3 fundamental of N_2O dissolved in hydrated DOPC bilayers were obtained to determine the lipid site dependence of VER. Magic-angle pump–probe studies were performed with 130 fs laser pulses tuned to the N_2O ν_3 absorption band. The dispersed probe transient response, reported as the pump-induced change in optical density (ΔOD) in the probe 2205 – 2245 cm^{-1} region, for a DOPC–water bilayer system with 20% H_2O by weight (~ 11 water molecules per DOPC, well below the excess water point) is shown in Figure 2A. This region of the transient spectrum is dominated by bleaching ($\Delta\text{OD} < 0$) because of pump-induced ground-state population loss and excited-state stimulated emission. The transient spectrum across the entire pulse spectrum (2160 – 2250 cm^{-1}) showing both bleach and excited-state absorption is included in the Supporting Information (Figure S1).

Single frequency fitting and multifrequency global analysis were employed to determine VER decay rates. Global analysis yields decay associated spectra (DAS) with corresponding lifetimes. Detailed discussion of data analysis procedures appears in the Experimental Procedures section. The dispersed transient spectrum for the 20% water DOPC sample is fit with two DAS (Figure 2B). Global fit attempts including additional components could not identify more than these two contributions. One DAS was centered at 2218 cm^{-1} and had a lifetime of $51 \pm 2 \text{ ps}$. Since these values are nearly identical to those obtained for N_2O in octanol and olive oil,³³ this component is attributed to N_2O solvated in acyl chain regions of the lipid. The second DAS is centered near 2230 cm^{-1} and decays in $29 \pm 2 \text{ ps}$. This absorption frequency is characteristic of N_2O in aqueous environments. However, the corresponding lifetime is a factor

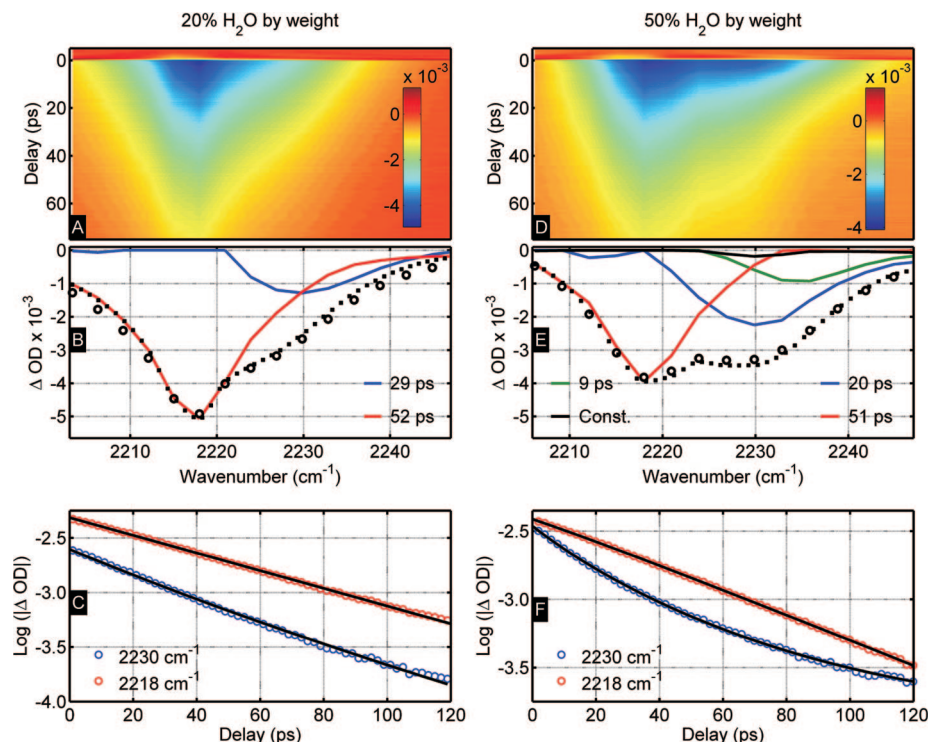


Figure 2. The pump-induced transient differential probe spectrum of N_2O in DOPC bilayers: (A) at 20% hydration and (D) at 50% hydration by weight. Corresponding decay associated spectra (DAS) obtained by global fitting analysis: (B) at 20% and (E) at 50% hydration systems. (B and E) The dotted black line is the sum of all DAS, and the black circles are the observed spectra at 200 fs. (C and F) Single wavelength slices of experimental (circles) and best-fit (black lines) results on a semilog plot. Single slices at the hydrophobic (2218 cm^{-1}) and hydrophilic (2230 cm^{-1}) sites of ν_3 absorption for (C) 20% and (F) 50% hydration DOPC.

of 3 longer than the N_2O ν_3 lifetime observed in bulk water (9 ± 2 ps) and is shorter than the hydrocarbon value (55 ± 2 ps). The hydration level of 20% is well below the excess water point for DOPC–water. Thus, this DAS is assigned to N_2O solvated in interlamellar water surrounding the polar head groups of the lipid.

The dispersed transient absorbance of the ν_3 band of N_2O (see Figure 2D) exhibits different VER kinetics in a 50% water–DOPC mixture (44 water molecules per lipid). This amount of water is well above the excess water point ($\sim 39\%$ by weight or 27 water molecules per lipid). In contrast to the 20% water–DOPC results, the global analysis requires additional components to fit the dispersed N_2O pump–probe transients in the more hydrated lipid (Figure 2E). A third DAS with a lifetime of 9 ± 2 ps is needed. This lifetime and frequency are consistent with the assignment of this DAS to N_2O dissolved in pools of bulk water. A constant DAS is also added to represent the sub-picosecond solvent heating contribution to the signal, which decays on a millisecond time scale and appears as a constant for the time range of these experiments (120 ps).⁴⁷

As a further test of the robustness of the global fit results, semilog plots of observed and best-fit single frequency slices for the 20% and 50% water–DOPC systems are shown in Figure 2C and 2F, respectively. A single 52 ps exponential decay provides an excellent fit to the 2218 cm^{-1} data slice, which is dominated by N_2O absorption in the lipid acyl chains for both samples. The 2230 cm^{-1} single frequency response of the 50% water–DOPC mixture, predominantly because of water-solvated N_2O , is best fit by a triexponential decay with time constants of 9, 20, and 51 ps in addition to a constant term to account for the solvent heating consistent with the global analysis described above. The 2230 cm^{-1} single slice response of the 20%

H_2O –DOPC lipid system is best fit with only a 20 ps decay and a small contribution of the 52 ps nonaqueous component. The inability of a biexponential model to fit the observed decay at 2230 cm^{-1} for the 50% water–DOPC system is demonstrated in Figure S3 in the Supporting Information. Fits to the data with stretched or power-law forms do not yield improved fits (see Figure S4). Results for the N_2O pump–probe response in DOPC at additional hydration levels (10%, 33%, 41%) are shown in the Supporting Information (Figures S2, S5–S7) as well. The center frequency of the DAS associated with the bulk waterlike 9 ps decay is slightly blue-shifted (Figure 2E). We attribute this frequency to the effects of local “heating” in bulk water which occurs on a sub-picosecond timescale and which decays slowly (ms).⁴⁷ Because of the difference in N_2O ν_3 and water spectral bandwidths in this region, most of the absorbed incident pulse energy is absorbed by the water. This blue-shifting effect as the temperature is increased is observed for the static FTIR spectrum of N_2O in water (see Figure S8 in Supporting Information).

The N_2O ν_3 lifetime components determined by this pump–probe analysis are plotted as a function of lipid hydration in Figure 3. The slowest component, associated with the 2218 cm^{-1} absorption band and characteristic of N_2O in the hydrocarbon tails, exhibits a lifetime of 51 ± 2 ps independent of hydration. However, the lifetime of the shorter lived component ($\sim 2230\text{ cm}^{-1}$) monotonically decreases from 43 ± 2 ps (10% H_2O , 5 water molecules per lipid) to 19 ± 2 ps (33% H_2O , 22 waters per lipid) until the excess water point (~ 27 water molecules per lipid)³ is reached (Figure 3). Above the excess water point, a third DAS near 2230 cm^{-1} with a lifetime of 9 ± 2 ps is required to fit the data and is assigned to the VER of N_2O in pools of bulklike water as discussed above. Thus, the

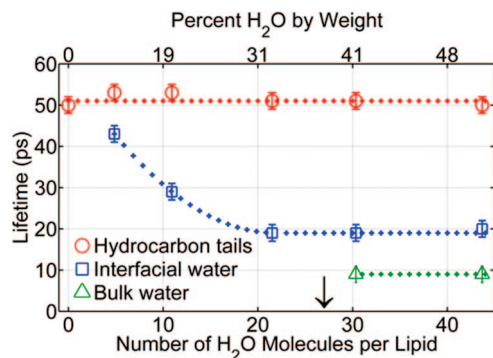


Figure 3. N_2O ν_3 lifetimes in the identified solvation environments (acyl chains, interfacial water, and bulk water pools) of hydrated DOPC bilayers as a function of hydration determined by IR pump–probe transient analysis. The black arrow indicates the excess water point for DOPC (27 water molecules per lipid).

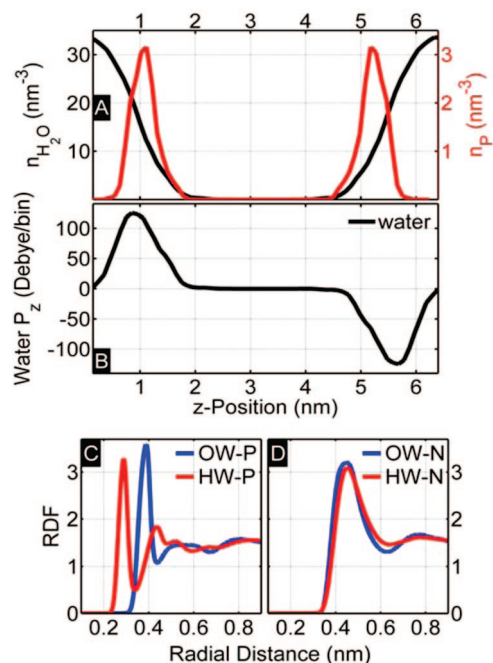


Figure 4. Simulation results for fully hydrated POPC bilayer. (A) Distribution of water number density per lipid and phosphorus number density as a function of distance along the normal to the lipid–water interface, z . (B) The z -component of water polarization, $\langle P_z \rangle$, as a function of z -position. (C) Radial distribution functions (RDFs) for the water oxygen (OW) and hydrogen (HW) atoms with respect to the POPC head group phosphorus. (D) RDFs for the water oxygen (OW) and hydrogen (HW) atoms with respect to the POPC head group nitrogen.

rate of N_2O VER is a sensitive function of the molecular composition and structure of the local lipid solvation environments.

Molecular Dynamics Simulations. The calculated density of water molecules ($n_{\text{H}_2\text{O}}$) and POPC head group phosphorus atoms (n_{P}) as a function of distance along the normal (z) to the lipid–water interface is shown in Figure 4A. The phospholipid head groups are centered at $z = 1.1$ nm and $z = 5.3$ nm in the interfacial water regions (Figure 4A). The bilayer acyl chains occupy the z -region from ~ 1.7 nm to ~ 4.7 nm. The time averaged z -component of the polarization due to water along the lipid–water interface normal, $\langle P_z \rangle$, shows positively and negatively peaked values at $z = 0.9$ and 5.5 nm in the interfacial water region (see Figure 4B). The anisotropic ordering of water molecules near the phosphatidylcholine head groups results in these nonzero values of $\langle P_z \rangle$.

Radial distribution functions (RDFs) between the oxygen and hydrogen atoms of the water molecules, and the anionic phosphate group phosphorus atom (OW-P, HW-P) and the cationic choline nitrogen atom (OW-N, HW-N) are shown in Figure 4C and 4D, respectively. As evident in these figures, the interfacial water molecules are strongly oriented, with one hydrogen atom of molecules in the first hydration shell being closer to the negatively charged phosphate groups. Virtually no water ordering is evident around the choline groups. This interfacial water molecules ordering accounts for the non-zero polarization $\langle P_z \rangle$ near the zwitterionic head groups.

Discussion

The VER of solute molecules in solvent is an area that has been subjected to intense attention in recent years.^{48–50} Elucidating the VER pathway for N_2O rigorously using theoretical modeling is by itself a major endeavor. For these one-color pump–probe studies of hydrated DOPC, we cannot determine the relative importance of intra- and intermolecular energy relaxation pathways for the return of the N_2O asymmetric vibrational level to equilibrium. However, for this simple triatomic linear molecule in solvents, we may assume that the VER results from ν_3 energy transfer to intermolecular modes. In bulk water, this can result from resonant energy transfer to the continuum of low-frequency H_2O vibrational states or the overlapping $\nu_{\text{B}} + \nu_{\text{L}}$ combination band in this spectral region (see Figure 1C). At 2230 cm^{-1} , the N_2O ν_3 transition frequency, both the continuum and the combination band make significant contributions to the water absorption intensity. In the hydrated lipid system, water molecules near the polar head group are strongly oriented as described above, and thus the normal H_2O hydrogen bonding network is altered. The disruption of the intermolecular structure is also evident in the low-frequency ($\leq 1000\text{ cm}^{-1}$) density of states calculated from the Fourier transformed velocity autocorrelation function. For example, calculated spectral densities⁵¹ for water molecules close to the phospholipid head group are significantly different than that of bulk water (see Figure S9).

Observed changes in the lipid-solvated water absorption spectrum are correlated with the N_2O vibrational decay effect described here for the interlamellar region. The normalized absorption intensity in the region of the $\nu_{\text{B}} + \nu_{\text{L}}$ water combination band of hydrated bilayers is shown as a function of lipid hydration in Figure 5A. The DOPC contributions to these spectra have been subtracted, and the resulting water spectra have been normalized by the number of water molecules in the hydrated lipid samples. As DOPC hydration increases from 10% to 33%, where the spectrum is exclusively due to interlamellar water molecules, the most significant change is the relative contribution of the continuum spectral density in this absorption region. The combination band intensity and shape, however, remain nearly constant. These two trends are indicated by the red and black lines, respectively, in Figure 5B. The ν_3 VER rates (inverse lifetimes) found for N_2O solvated in interfacial water environments are shown in this figure as well (blue line). Below 33% hydration, the VER of N_2O shows a strong dependence on hydration level as does the continuum contribution to the IR spectral density (Figure 5B). At greater hydration levels, where pools of bulk water form, the absorption spectrum due to both the combination band and the underlying continuum in this region shows relatively little change (Figure 5A and 5B). Correspondingly, the observed ν_3 N_2O lifetime exhibits a constant ~ 20 ps decay and a second component with characteristics of N_2O in bulk water. These results suggest that

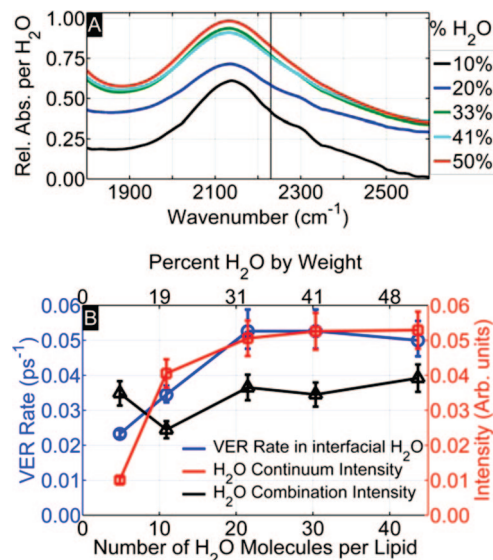


Figure 5. (A) FTIR of the water combination band region in hydrated DOPC bilayers normalized by relative water concentration as a function of hydration level (% weight of H₂O). Residual DOPC absorption background has been removed. (B) Plot of N₂O ν_3 VER rates (inverse lifetime) in interfacial water regions of hydrated DOPC (blue). Relative H₂O continuum (red) and $\nu_{\text{bending}} + \nu_{\text{vibration}}$ combination band (black) absorption intensity at 2230 cm⁻¹ as a function of hydration.

the rate of ν_3 N₂O VER in aqueous environments results from energy transfer preferentially to the continuum of water states resonant with the ν_3 band as compared to the $\nu_B + \nu_L$ combination band.

Furthermore, MD simulations revealed a perturbed hydrogen bonding network of the oriented water molecules near the phospholipid head group as evidenced by ordered water arrangement (Figure 4) and a shift in the intermolecular vibrational spectrum for water molecules near the phospholipid head groups (Figure S9). As has been well established, the rate of vibrational energy relaxation is proportional to the density of energy-receiving states.^{18,52,53} Thus, the observed slower rates of energy transfer from N₂O in the interfacial water molecules is attributed to the reduced density of continuum states evident in this region of the lipid–water spectrum (Figure 5A). In addition, the coupling to these low-frequency bath modes may also be affected and may contribute to the observed hydration level dependence of the ν_3 VER. In contrast, N₂O ν_3 VER in the hydrophobic phospholipid site is the slowest where no equivalent solvent density of states is evident. More detailed calculations will be required to help verify the nature of this proposed VER mechanism. With the use of an appropriately designed thin sample cell, the ability to observe changes in hydrogen bonding⁵⁴ via the OH stretch absorption region could provide additional information on the nature of these interlamellar water molecules that account for the reported N₂O lifetime effects.

Conclusion

Our results demonstrate that the lifetime of the ν_3 fundamental of dissolved N₂O is sensitive to solvation environments in hydrated phospholipids revealing hydrophobic as well as interfacial and bulk water sites. While it is well-known that rates of VER are sensitively solvent dependent and hence indirect measures of local environments, the unique finding demonstrated here is that VER from a solute (N₂O) to a single solvent (H₂O) varies continuously as a function of the changing ordered solvent

environment. The nonbulk structure of the “special” interfacial biological water results in a greatly reduced spectral density in the 2200 cm⁻¹ region. In order to further develop N₂O VER as a probe of interfacial water, a more detailed molecular level description of the structure and dynamics of water molecules perturbed by the phospholipid head group is required. This analysis can be aided both by time-resolved anisotropy and ultrafast 2-dimensional infrared measurements of the ν_3 N₂O band.

Orientational ordering of interfacial water molecules occurs not only in lipid membranes but in nucleic acid and protein structures as well. The N₂O VER site dependence also suggests that ultrafast IR spectroscopy may be a useful experimental approach for learning about the molecular sites responsible for the anesthetic action of N₂O.^{26,28–30,55} For example, it has been proposed that the disruption of hydrogen bonds in special lipid interfacial water molecules is implicated in anesthetic action.^{30,56} Alternatively, the anesthetic activity of N₂O has been proposed to arise from protein pocket sites, which may be hydrophobic or hydrophilic.^{26,28,29,55} Thus, the use of this N₂O vibrational energy transfer as a probe of interfacial water molecules in these additional biological structures appears promising.

Acknowledgment. The support of the National Science Foundation (LDZ, CHE-0310497; EP, DGE-0221680) and the Boston University Photonics Center is gratefully acknowledged.

Supporting Information Available: Figures S1–S9 as defined in the text. This information is available free of charge via the Internet at <http://pubs.acs.org>.

References and Notes

- (1) Milhaud, J. *Biochim. Biophys. Acta* **2004**, *1663*, 19.
- (2) Gawrisch, K.; Ruston, D.; Zimmerberg, J.; Parsegian, V. A.; Rand, R. P.; Fuller, N. *Biophys. J.* **1992**, *61*, 1213.
- (3) Hristova, K.; White, S. H. *Biophys. J.* **1998**, *74*, 2419.
- (4) Fitter, J.; Lechner, R. E.; Dencher, N. A. *J. Phys. Chem. B* **1999**, *103*, 8036.
- (5) Jurkiewicz, P.; Sykora, J.; Olzynska, A.; Humpolickova, J.; Hof, M. *J. Fluoresc.* **2005**, *15*, 883.
- (6) Kim, J.; Lu, W.; Qiu, W.; Wang, L.; Caffrey, M.; Zhong, D. *J. Phys. Chem.* **2006**, *110*, 21994.
- (7) Cheng, J. X.; Pautot, S.; Weitz, D. A.; Xie, X. S. *Proc. Natl. Acad. Sci. U.S.A.* **2003**, *100*, 9826.
- (8) Bursing, H.; Ouw, D.; Kundu, S.; Vohringer, P. *Phys. Chem. Chem. Phys.* **2001**, *3*, 2378.
- (9) Alper, H. E.; Bassolinoklimas, D.; Stouch, T. R. *J. Chem. Phys.* **1993**, *99*, 5547.
- (10) Tieleman, D. P.; Marrink, S. J.; Berendsen, H. J. *Biochim. Biophys. Acta* **1997**, *1331*, 235.
- (11) Murzyn, K.; Zhao, W.; Karttunen, M.; Kurdziel, M.; Rog, T. *Biointerphases* **2006**, *1*, 98.
- (12) Levinger, N. E. *Sciences (NY)* **2002**, *298*, 1722.
- (13) Sando, G. M.; Dahl, K.; Zhong, Q.; Owrutsky, J. C. *J. Phys. Chem.* **2005**, *109*, 5788.
- (14) Tan, H. S.; Piletic, I. R.; Fayer, M. D. *J. Chem. Phys.* **2005**, *122*.
- (15) Piletic, I. R.; Tan, H. S.; Fayer, M. D. *J. Phys. Chem. B* **2005**, *109*, 21273.
- (16) Cringus, D.; Lindner, J.; Milder, M. T. W.; Pshenichnikov, M. S.; Vohringer, P.; Wiersma, D. A. *Chem. Phys. Lett.* **2005**, *408*, 162.
- (17) Dokter, A. M.; Woutersen, S.; Bakker, H. J. *Phys. Rev. Lett.* **2005**, *94*.
- (18) Owrutsky, J. C.; Raftery, D.; Hochstrasser, R. M. *Annu. Rev. Phys. Chem.* **1994**, *45*, 519.
- (19) Herzberg, G. *Infrared and Raman Spectra*; Van Nostrand: Princeton, NJ, 1967.
- (20) Lapinski, A.; Spanget-Larsen, J.; Waluk, J.; Radziszewski, J. *J. Chem. Phys.* **2001**, *115*, 1757.
- (21) Tidwell, E. D.; Plyler, E. K.; Benedict, W. S. *J. Opt. Soc. Am.* **1960**, *50*, 1243.
- (22) Burch, D. E.; Williams, D. *Appl. Opt.* **1960**, *1*, 473.
- (23) Shulman, R. G.; Dailey, B. P.; Townes, C. H. *Phys. Rev.* **1950**, *78*, 145.

- (24) Janoff, A. S.; Miller, K. W. In *Biological Membranes*; Chapman, D., Ed.; Academic Press: London, 1982; p 417.
- (25) Urban, B. W.; Bleckwenn, M.; Barann, M. *Pharmacol. Ther.* **2006**, *111*, 729.
- (26) Franks, N. P.; Lieb, W. R. *Nature* **1982**, *300*, 487.
- (27) Gruner, S. M.; Shyamsunder, E. *Ann. N.Y. Acad. Sci.* **1991**, *625*, 685.
- (28) Franks, N. P.; Lieb, W. R. *Nature* **1994**, *367*, 607.
- (29) Jevtic-Todorovic, V.; Todorovic, S. M.; Mennerick, S.; Powell, S.; Dikranian, K.; Benshoff, N.; Zorumski, C. F.; Olney, J. W. *Nat. Med.* **1998**, *4*, 460.
- (30) Chiou, J. S.; Ma, S. M.; Kamaya, H.; Ueda, I. *Science* **1990**, *248*, 583.
- (31) Gorga, J. C.; Hazzard, J. H.; Caughey, W. S. *Arch. Biochem. Biophys.* **1985**, *240*, 734.
- (32) Dong, A.; Huang, P.; Zhao, X. J.; Sampath, V.; Caughey, W. S. *J. Biol. Chem.* **1994**, *269*, 23911.
- (33) Chieffo, L.; Amsden, J.; Shattuck, J.; Hong, M. K.; Ziegler, L.; Erramilli, S. *Biophys. Rev. Lett.* **2006**, *1*, 309.
- (34) Chieffo, L.; Shattuck, J.; Amsden, J. J.; Hong, M. K.; Erramilli, S.; Ziegler, L. D. Femtosecond infrared spectroscopy of molecular probes of anesthetic action. *234th American Chemical Society National Meeting*, Boston, MA, 2007.
- (35) Hamm, P.; Lim, M.; Hochstrasser, R. M. Vibrational relaxation and dephasing of small molecules strongly interacting with water. *Ultrafast Phenomena XI: Proceedings of the 11th International Conference*, Garmisch-Partenkirchen, Germany, 1998.
- (36) van Stokkum, I. H.; Larsen, D. S.; van Grondelle, R. *Biochim. Biophys. Acta* **2004**, *1657*, 82.
- (37) Rosenfeld, D. E.; Schmittenmaier, C. A. *J. Phys. Chem. B* **2006**, *110*, 14304.
- (38) Viecelli, J.; Chorny, I.; Benjamin, I. *J. Chem. Phys.* **2002**, *117*, 4532.
- (39) Bhide, S. Y.; Berkowitz, M. L. *J. Chem. Phys.* **2005**, *123*, 224702.
- (40) Mashl, R. J.; Scott, H. L.; Subramaniam, S.; Jakobsson, E. *Biophys. J.* **2001**, *81*, 3005.
- (41) Wu, Y.; Tepper, H. L.; Voth, G. A. *J. Chem. Phys.* **2006**, *124*, 024503.
- (42) Lindahl, E.; Hess, B.; van der Spoel, D. *J. Mol. Model.* **2001**, *7*, 306.
- (43) Berendsen, H. J. C.; Vanderspoel, D.; Vandrunen, R. *Comput. Phys. Commun.* **1995**, *91*, 43.
- (44) Ryckaert, J. P.; Ciccotti, G.; Berendsen, H. J. C. *J. Comput. Phys.* **1977**, *23*, 327.
- (45) http://moose.bio.ucalgary.ca/index.php?page=Structures_and_Topologies (accessed January 14, 2008).
- (46) Essmann, U.; Perera, L.; Berkowitz, M. L.; Darden, T.; Lee, H.; Pedersen, L. G. *J. Chem. Phys.* **1995**, *103*, 8577.
- (47) Chieffo, L.; Shattuck, J.; Amsden, J. J.; Erramilli, S.; Ziegler, L. D. *Chem. Phys.* **2007**, *341*, 71.
- (48) Fujisaki, H.; Zhang, Y.; Straub, J. E. *J. Chem. Phys.* **2006**, *124*, 144910.
- (49) Morita, A.; Kato, S. *J. Chem. Phys.* **1998**, *109*, 5511.
- (50) Garcia-Viloca, M.; Nam, K.; Alhambra, C.; Gao, J. *J. Phys. Chem. B* **2004**, *108*, 13501.
- (51) McQuarrie, D. A. *Statistical Mechanics*; University Science Books: Sausalito, CA, 2000.
- (52) Oxtoby, D. W. *Adv. Chem. Phys.* **1981**, *47*.
- (53) Aubuchon, C. M.; Rector, K. D.; Holmes, W.; Fayer, M. D. *Chem. Phys. Lett.* **1999**, *299*, 84.
- (54) Binder, H. *Eur. Biophys. J.* **2007**, *36*, 265.
- (55) Abraham, M. H.; Lieb, W. R.; Franks, N. P. *J. Pharm. Sci.* **1991**, *80*, 719.
- (56) Tang, P.; Xu, Y. *Proc. Natl. Acad. Sci. U.S.A.* **2002**, *99*, 16035.

JP8012283